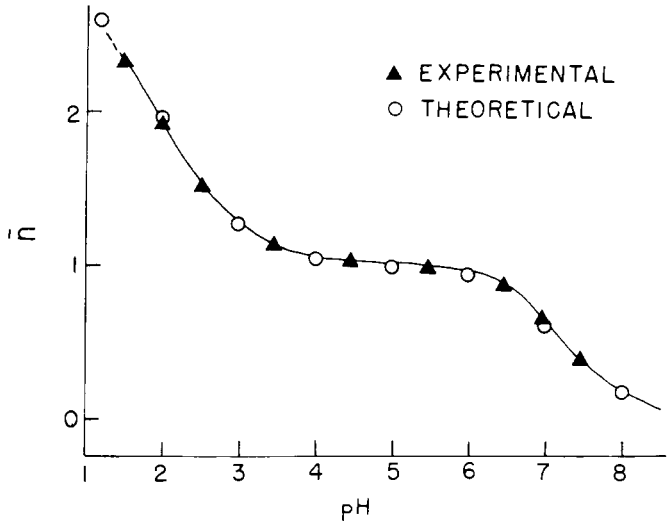

Figure 2. Experimental and theoretical proton dissociation curves for 2,2′-iminodimethylene dipyridine

respectively). The temporary values were then refined to obtain the stepwise constants with one part per thousand agreement. The reliability of the final stepwise pK_n's was confirmed by generation of a theoretical dissociation curve as shown in Figure 2. The final stepwise values were $pK_1 = 7.30 \pm 0.02$, $pK_2 = 2.60 \pm 0.02$, and $pK_3 = 1.12 \pm 0.04$.

ACKNOWLEDGMENT

Appreciation is expressed to C. C. Cheng and Scott Searles, Jr., for their advice and to John A. Landgrebe for NMR spectra.

LITERATURE CITED

(1) Bjerrum, J., "Metal Amine Formation in Aqueous Solution," P. Haase and Son, Copenhagen, 1957.
(2) Hoyer, E., *Chem. Ber.* **93**, 2475 (1960).
(3) Huber, W., *J. Am. Chem. Soc.* **66**, 876 (1944).
(4) Lacoste, R.G., Martell, A.E., *Inorg. Chem.* **3**, 881 (1964).
(5) Martell, A.E., Calvin, M., "Chemistry of the Metal Chelate Compounds," Prentice-Hall, Englewood Cliffs, N.J., 1952.
(6) Osuch, C., Levine, R., *J. Am. Chem. Soc.* **78**, 1723 (1956).
(7) Romary, J.K., Andrews, A.C., Division of Analytical Chemistry, Winter Meeting, ACS, Phoenix, Ariz., January 1966.

RECEIVED for review August 11, 1966. Accepted December 17, 1966. The authors gratefully acknowledge the support of this research by the donors of The Petroleum Research Fund, administered by the American Chemical Society (Grant 2185-B) and by the National Science Foundation (Grants GE-6492 and GY-274).

Graphical Determination of Virial Coefficients by the Burnett Method

Isopentane and Neopentane

I. H. SILBERBERG
Texas Petroleum Research Committee, Austin, Tex.
DAVID C.K. LIN and J. J. McKETTA
Department of Chemical Engineering, University of Texas, Austin, Tex.

A new graphical analysis has been developed for data obtained from the Burnett method of compressibility measurement. This method of analysis, based upon the Leiden virial equation of state, permits accurate determination of the second and third virial coefficients as well as the gas density at the initial pressure in the series of expansions. If the experimental data are sufficiently precise, fourth virial coefficients may also be obtained. In this paper, the method is applied to data on isopentane and neopentane from 30° to 200° C.

SINCE its introduction 30 years ago, the Burnett method (*2*) of gas compressibility measurement has slowly but steadily increased in importance as a rapid means of obtaining vapor phase PVT data with high precision. The method has been used from temperatures as low as −140° C. (*4, 5*) to as high as 1200° C. (*12*) and at pressures ranging from sub-atmospheric (*6*) to greater than 525 atm. (*4, 5*). The method has been employed with gases of extremely high purity, with binary gas mixtures, and with multicomponent (natural) gas mixtures. At the present time, a number of Burnett apparatus research projects are known to be active in the United States.

Investigators in the past have generally analyzed Burnett experimental data either graphically to give compressibility factors or analytically, assuming some form of an equation of state, to give virial or virial-type coefficients. Both graphical and analytical methods were discussed in detail in an earlier paper (*10*). The purpose of the present paper is to introduce a new method of graphical analysis capable of generating second, third, and (with sufficiently precise

experimental data) even fourth virial coefficients from original, unprocessed data obtained by the Burnett method. A further benefit of the method is improved accuracy in the compressibility factor isotherms themselves.

BURNETT METHOD

The original Burnett apparatus consisted of a measuring chamber and an expansion chamber, the volumes of which are independent of pressure. Both chambers are maintained at the same, constant temperature. The measuring chamber is filled to some unknown density, ρ_0, with the experimental gas, and the initial pressure, p_0, is measured. The gas is then expanded through an interconnecting valve to the previously evacuated expansion chamber. When thermal equilibrium is restored, the expansion valve is closed and another pressure, p_1, is measured. The contents of the expansion chamber are then discarded and the process repeated. In this manner a series of isothermal pressures is obtained: $p_0, p_1, \ldots, p_r, \ldots, p_f$. The final pressure, p_f, is generally the lowest pressure that can be measured with adequate accuracy.

Modifications of this basic method have included: use of expansion chambers to allow a choice of the density decrement with each expansion (*8*), treatment of chamber volumes as functions of pressure (*4, 5*), and measuring and expansion chambers maintained at constant but different temperatures (*12*). In the development presented here, it will be assumed that all chambers are maintained at the same temperature.

The apparatus constant is defined as the ratio of the system volume after the expansion to that before the expansion; this is in general represented by N_r. The density before the rth expansion ρ_{r-1} and the density after the rth expansion ρ_r are related by the following:

$$\rho_r = \rho_{r-1}/N_r \; (r = 1, 2, \ldots, f) \tag{1}$$

When the compressibility factor $z = p/\rho RT$ is introduced into Equation 1, there results

$$\frac{p_{r-1}/T_{r-1}}{p_r/T_r} = \frac{z_{r-1}}{z_r} N_r \tag{2}$$

The temperatures T_{r-1} and T_r have been retained to account for possible minor variations in temperature from expansion to expansion. Equation 2 is useful for the evaluation of N_∞, the limiting value of the apparatus constant as the pressure approaches zero. Since the compressibility factor approaches unity as pressure approaches zero,

$$\underset{p_r \to 0}{\text{Limit}} \frac{p_{r-1}/T_{r-1}}{p_r/T_r} = \underset{p_{r-1} \to 0}{\text{Limit}} \frac{p_{r-1}/T_{r-1}}{p_r/T_r} = N_\infty \tag{3}$$

Equation 3 is the basis for the graphical method of determining the basic apparatus constant. The method has been discussed in detail in an earlier paper (*10*).

Repetitive application of Equation 1 leads to the following relation:

$$\rho_r = \rho_0 \prod_{i=1}^{r} N_i^{-1} = \rho_0 \pi_r^{-1} \tag{4}$$

where ρ_0 is the initial molal density for the series of expansions. Introducing the compressibility factor into Equation 4 leads to

$$\frac{p_r}{RT_r} \pi_r = \frac{p_0}{z_0 RT_0} z_r = \rho_0 z_r \tag{5}$$

from which it follows that

$$\underset{p_r \to 0}{\text{Limit}} \frac{p_r}{RT_r} \pi_r = \rho_0 \tag{6}$$

Equation 6 is the basis for the graphical determination of the initial density, ρ_0, by extrapolation to zero pressure, as illustrated by the Berlin curve in Figure 1. This technique for determining ρ_0 might be called the Berlin method. With this value for ρ_0, values of the compressibility factor, z_r, at the various p_r are easily calculated from a rearrangement of Equation 5.

VIRIAL COEFFICIENTS

The virial equation of state, also called the Leiden equation, is written as

$$z = p/\rho RT = 1 + B\rho + C\rho^2 + D\rho^3 + \ldots \tag{7}$$

in which B, C, and D are the second, third, and fourth virial coefficients, respectively. Since pressure rather than density is measured in the Burnett method, many previous investigators have concluded that Equation 7 cannot be used directly to analyze the data from a series of expansions (a run) in a Burnett apparatus. Consequently, the so-called Berlin equation of state has commonly been employed for both graphical and analytical treatments of the experimental data.

$$z = 1 + B'p + C'p^2 + D'p^3 + \ldots \tag{8}$$

The virial-type coefficients B', C', and D' may be related to the virial coefficients for the case in which Equations 7 and 8 are both infinite series. Equation 8 generally does not converge so rapidly as does Equation 7; in other words, the graph of z *vs.* ρ generally exhibits less curvature than does the graph of z *vs.* p.

Silberberg, Kobe, and McKetta (*10*) indicated a method whereby original experimental data from a Burnett apparatus might be treated analytically according to Equation 7. Least squares values for the virial coefficients as well as for the apparatus constant and the initial density could be obtained in an iterative procedure. The following development will reveal that a graphical method, involving first and second residuals, can similarly be employed directly with the experimental data (p_r, T_r) to yield the initial density and second, third, and fourth virial coefficients, provided that the apparatus constant is accurately known.

NEW METHOD

Equation 7 may be rewritten as

$$p/RT = \rho + B\rho^2 + C\rho^3 + D\rho^4 + \ldots \tag{9}$$

Applying this equation to the state of the system after the rth expansion, there results

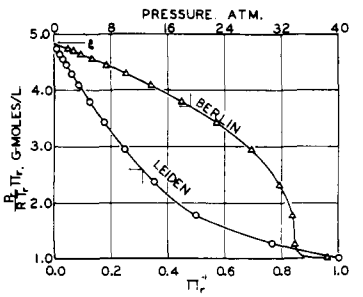

Figure 1. Comparison of Leiden and Berlin methods

Isopentane at 188.5° C. run No. 41, data of Silberberg (*11*)

$$\frac{p_r}{RT_r} = \rho_r + B_r\rho_r^2 + C_r\rho_r^3 + D_r\rho_r^4 + \ldots \qquad (10)$$

where

$B_r = B(T_r)$, the second virial coefficient at T_r

$C_r = C(T_r)$, the third virial coefficient at T_r

$D_r = D(T_r)$, the fourth virial coefficient at T_r

Combining Equations 4 and 10 results in

$$\frac{p_r}{RT_r}\pi_r = \rho_0 + B_r\rho_0^2\pi_r^{-1} + C_r\rho_0^3\pi_r^{-2} + D_r\rho_0^4\pi_r^{-3} + \ldots \qquad (11)$$

If the temperatures T_1, T_2, ..., T_f vary only slightly, the effect on B, C, and D may be neglected and these virial coefficients replaced by single values at the average temperature.

$$\frac{p_r}{RT_r}\pi_r = \rho_0 + B\rho_0^2\pi_r^{-1} + C\rho_0^3\pi_r^{-2} + D\rho_0^4\pi_r^{-3} + \ldots \qquad (12)$$

Equation 12 indicates that, if $p_r\pi_r/RT_r$ is plotted against π_r^{-1}, the zero-abscissa intercept is the initial density, ρ_0, and the slope at the intercept is $B\rho_0^2$, permitting calculation of the second virial coefficient. Since the Leiden virial equation generally converges more rapidly than the Berlin equation, this Leiden method should result in a graph with less curvature and afford greater accuracy in determining ρ_0 than the Berlin method. This fact is clearly illustrated in Figure 1. The Leiden method of determining ρ_0 is also illustrated by the curves marked *a* in Figures 2 and 3. However, a still more sensitive method is described in the next section.

The independent variable in Equation 12, π_r^{-1}, is nothing more than a reduced density, that is, the density at pressure p_r is divided by the initial density of the run. Hence, the values of π_r^{-1} always lie between zero and one. Another interesting property of π_r^{-1} is the fact that it should not contain appreciable random errors, although systematic errors may be present from either the calibration to determine N_∞ or the correction for pressure.

For the special case in which $N_1 = N_2 = \ldots = N_f = N$, $\pi_r = N^r$ and Equation 12 becomes simply

$$\frac{p_rN^r}{RT_r} = \rho_0 + B\rho_0^2N^{-r} + C\rho_0^3N^{-2r} + D\rho_0^4N^{-3r} + \ldots \qquad (13)$$

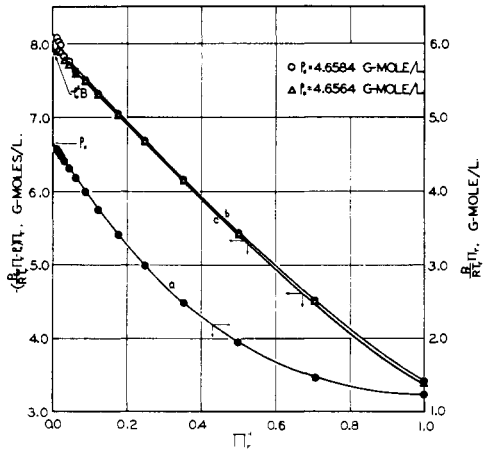

Figure 2. Determination of the virial coefficients of isopentane at 200° C.
Run No. 38, data of Silberberg (*11*)

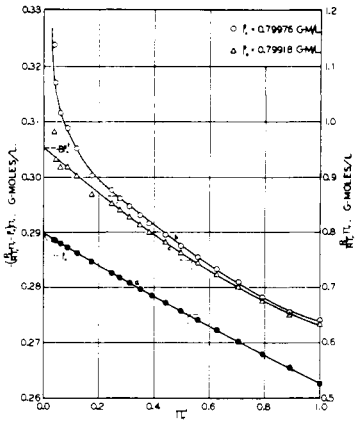

Figure 3. Determination of the virial coefficients of neopentane at 125° C.
Run No. 11, data of Heichelheim (*8*)

For such a case, the graph of p_rN^r/RT_r *vs.* N^{-r} will have a zero-abscissa intercept of ρ_0 and a slope at the intercept of $B\rho_0^2$. Furthermore, regardless of the initial density and even the identity of the experimental gas, the set of values of the independent variable N^{-r} will remain constant so long as N is unchanged.

The state of the system before the rth expansion is described similarly by

$$\frac{p_{r-1}N^{r-1}}{RT_{r-1}} = \rho_0 + B\rho_0^2N^{-(r-1)} + C\rho_0^3N^{-2(r-1)} + D\rho_0^4N^{-3(r-1)} + \ldots \qquad (14)$$

If Equations 13 and 14 are combined, the following relation results:

$$N^{2r}\left(N\frac{p_r}{T_r} - \frac{p_{r-1}}{T_{r-1}}\right) = BRN(1-N)\rho_0^2 + CRN(1-N^2)\rho_0^3N^{-r} + DRN(1-N^3)\rho_0^4N^{-2r} + \ldots \qquad (15)$$

For the data of a single run, Equation 15 takes the form of

$$N^{2r}\left(N\frac{p_r}{T_r} - \frac{p_{r-1}}{T_{r-1}}\right) = b + cN^{-r} + dN^{-2r} + \ldots \qquad (16)$$

in which b, c, and d are constants. Therefore, the residual quantity on the left may be plotted against N^{-r} to give a graph which tends ever more toward linearity as r increases, that is, as N^{-r} approaches zero. This relationship provides a sensitive test of the value of N employed, and in fact offers a procedure for determining N which is alternative to that represented by Equation 3. This technique has been employed by Butcher and Dadson (*3*) and is illustrated here in Figure 10 in the Appendix.

FIRST RESIDUAL DATA PLOTS

A commonly used technique in the graphical treatment of data is to reduce the range of the dependent variable. Some other quantity, which varies with the independent variable in approximately the same manner or which the dependent variable approaches as a limit, is subtracted from its values. Such a residual type of function can easily be formed by rearrangement of Equation 12.

$$\left(\frac{p_r\pi_r}{RT_r} - \rho_0\right)\pi_r = B\rho_0^2 + C\rho_0^3\pi_r^{-1} + D\rho_0^4\pi_r^{-2}\ldots \qquad (17)$$

Equation 17 may also be written as

$$\left(\frac{p_r\pi_r}{RT_r} - \rho_0\right)\pi_r\rho_0^{-2} = B + C\rho_0\pi_r^{-1} + D\rho_0^2\pi_r^{-2} + \ldots \qquad (18)$$

Equation 17 offers a very sensitive means for trial-and-error determination of the correct value of ρ_0 from the experimental data of a run. As r increases (additional expansions), π_r increases and $p_r\pi_r/RT_r$ approaches ρ_0 more closely, as is shown by Equation 12. Therefore, the value of the left side of Equation 17 becomes quite sensitive to assumed values of ρ_0. Since the equation predicts a graph which tends to become linear as π_r^{-1} decreases, and since the spacing of the values of π_r^{-1} along the abscissa also decreases, the departure of the data points from linearity at these low values of reduced density is quite marked. The best value of ρ_0 is that which gives the most nearly linear trend of the data points as the density decreases. However, since this is a residual treatment of the data, small random errors in p_r at these points introduce relatively large deviations in the graph, with the result that an occasional low-pressure data point must be ignored in the analysis.

Figures 2 and 3 illustrate this technique. In Figure 2, curve b is based on the value of ρ_0 determined for isopentane by Silberberg, McKetta, and Kobe (*11*) from a plot of only the low-pressure data using the Berlin method. The slight curvature at low density indicates the value of ρ_0 was too high; use of a value approximately 0.04% lower resulted in the improved linearity of curve c. The effect of 0.07% error in ρ_0 is shown in Figure 3, based on the neopentane data of Heichelheim and coworkers (*8*). The value of ρ_0 = 0.79976 gram mole per liter determined by Heichelheim using the Berlin method is clearly too high. In both cases, the sensitivity of the residual plot to the value of ρ_0 provides far greater accuracy in ρ_0 than could be obtained by large-scale Leiden method plots of the data as illustrated by the curves marked a.

From Equations 17 and 18, the following observations may be made:

$$\underset{\pi_r^{-1}\to 0}{\text{Limit}} \left[\left(\frac{p_r\pi_r}{RT_r} - \rho_0\right)\pi_r\right] = B\rho_0^2 \tag{19}$$

$$\underset{\pi_r^{-1}\to 0}{\text{Limit}} \left[\left(\frac{p_r\pi_r}{RT_r} - \rho_0\right)\pi_r\rho_0^{-2}\right] = B \tag{20}$$

$$\underset{\pi_r^{-1}\to 0}{\text{Limit}} \frac{d}{d\pi_r^{-1}} \left[\left(\frac{p_r\pi_r}{RT_r} - \rho_0\right)\pi_r\right] = C\rho_0^3 \tag{21}$$

$$\underset{\pi_r^{-1}\to 0}{\text{Limit}} \frac{d}{d\pi_r^{-1}} \left[\left(\frac{p_r\pi_r}{RT_r} - \rho_0\right)\pi_r\rho_0^{-2}\right] = C\rho_0 \tag{22}$$

Equations 19 and 21 indicate that plotting the left side of Equation 17 *vs.* π_r^{-1} will give a graph with an intercept of $B\rho_0^2$ and a slope at the intercept of $C\rho_0^3$ (Figures 2 and 3). Therefore, for the same gas at the same temperature, each series of expansions started from a different initial density will give a different intercept and a different slope at the intercept. On the other hand, Equations 20 and 22 indicate that plotting the left side of Equation 18 *vs.* π_r^{-1} will, for runs at the same temperature but with different initial densities, give the same intercept but different slopes at the intercept. This feature of the new method is illustrated in Figure 4, in which run No. 38A is actually the last nine points of run No. 38, treated as if they constituted a separate run.

SECOND RESIDUAL DATA PLOTS

A second residual function may be created from Equation 17 by rearrangement.

$$\left[\left(\frac{p_r\pi_r}{RT_r} - \rho_0\right)\pi_r - B\rho_0^2\right]\pi_r = C\rho_0^3 + D\rho_0^4\pi_r^{-1} + \ldots \tag{23}$$

Equation 23 may also be written as

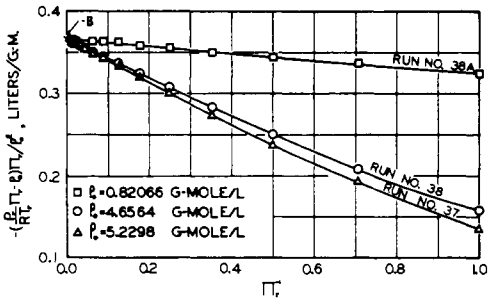

Figure 4. Consistency of the virial coefficients of isopentane at 200° C.
Data of Silberberg (*11*)

$$\left[\left(\frac{p_r\pi_r}{RT_r} - \rho_0\right)\pi_r - B\rho_0^2\right]\pi_r\rho_0^{-3} = C + D\rho_0\pi_r^{-1} + \ldots \tag{24}$$

These equations require a knowledge of ρ_0, determined from the first residual plot, and permit a trial-and-error determination of B as that value which gives the most linear trend when the left side of either equation is plotted *vs.* π_r^{-1}. This second residual function will be very sensitive to the assumed value of B. However, this same sensitivity will cause wide scattering of the low-density data points unless extremely high precision of measurement was maintained. Fortunately, the second residual plot will possess less curvature than the first, so that the loss of the low-density data points is not generally serious.

From Equations 23 and 24, the following observations are easily made:

$$\underset{\pi_r^{-1}\to 0}{\text{Limit}} \left[\left(\frac{p_r\pi_r}{RT_r} - \rho_0\right)\pi_r - B\rho_0^2\right]\pi_r = C\rho_0^3 \tag{25}$$

$$\underset{\pi_r^{-1}\to 0}{\text{Limit}} \left[\left(\frac{p_r\pi_r}{RT_r} - \rho_0\right)\pi_r - B\rho_0^2\right]\pi_r\rho_0^{-3} = C \tag{26}$$

$$\underset{\pi_r^{-1}\to 0}{\text{Limit}} \frac{d}{d\pi_r^{-1}} \left\{\left[\left(\frac{p_r\pi_r}{RT_r} - \rho_0\right)\pi_r - B\rho_0^2\right]\pi_r\right\} = D\rho_0^4 \tag{27}$$

$$\underset{\pi_r^{-1}\to 0}{\text{Limit}} \frac{d}{d\pi_r^{-1}} \left\{\left[\left(\frac{p_r\pi_r}{RT_r} - \rho_0\right)\pi_r - B\rho_0^2\right]\pi_r\rho_0^{-3}\right\} = D\rho_0 \tag{28}$$

Equations 25 and 27 show that plotting the left side of Equation 23 against π_r^{-1} will give a graph with an intercept of $C\rho_0^3$ and a slope at the intercept of $D\rho_0^4$. For the same gas at the same temperature, the data from each run with a different initial density would give a different intercept and a different slope at the intercept. On the other hand, Equations 26 and 28 indicate that plotting the left side of Equation 24 *vs.* π_r^{-1} will, for runs at the same temperature but with different initial densities, give the same intercept but different slopes at the intercept (Figure 5).

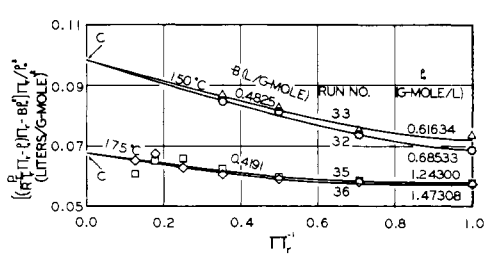

Figure 5. Determination of the virial coefficients of isopentane by the second residual method
Data of Silberberg (*11*)

APPLICATIONS

Isopentane. Twenty of the Burnett apparatus runs with isopentane reported by Silberberg, McKetta, and Kobe (*11*) were analyzed by this new method. The temperature range of these runs was from 50° to 200° C. and included two runs at 188.5° C., slightly above the critical temperature. The results of the first residual treatment are shown in Table I; the apparatus constant used was that reported by Silberberg. Because of the trial-and-error procedure with respect to ρ_0, it was more convenient to analyze each run separately according to Equation 17 (Figure 2). Therefore, some minor differences exist in Table I between second virial coefficients, determined according to Equation 19, reported for runs at the same temperature. Agreement of the third virial coefficient values from runs at the same temperature, determined according to Equation 21, is also very good.

Arithmetic average values of the second and third virial coefficients at each temperature are plotted in Figure 6. Also shown in that same figure are the values of B derived from the same data by Silberberg, McKetta, and Kobe (*11*), using extrapolations of isothermal residual volumes, $RT/p - V$, to zero pressure, as well as the few values reported by Scott *et al.* (*9*). The results of the new method of analysis for B differ from those of the earlier treatment by from 2 to 16 ml. per gram mole. Consistency with the values reported by Scott and coworkers (*9*) is excellent.

Also in Table I is a comparison between values of the initial density ρ_0 determined in this work with those reported by Silberberg, McKetta, and Kobe (*11*), which were determined as intercepts from large-scale Berlin-type plots (Figure 1) of the low-pressure data. Deviations between the two sets of results do not exceed 0.07%, the values of ρ_0 from a new method of analysis being consistently smaller than those reported by Silberberg. The average deviation is about 0.04%. Therefore, compressibility factors reported in the earlier paper would appear to be slightly too great, but the error is well within the estimated uncertainties of that work.

Thirteen of the isopentane runs were analyzed by the second residual treatment according to Equation 24 (Figure 5). Because of the greater sensitivity of the second residual to random errors, all runs at 50° and 75° C., as well as one run each at 125°, 150°, and 175° C., had to be rejected. In theory, B could possibly have been determined by trial-and-error procedures, as outlined earlier. However, the precision of the data did not warrant this technique. Therefore, the values of B employed were those (Table II) which were read from the smoothed graph of B *vs.* temperature (Figure 6). Severe scattering of low-pressure data necessitated disregarding all points below approximately 5 atm. The value of the third virial coefficient, C, was obtained at each temperature from the common intercept of the second residual curves (Equation 28). Third and fourth virial coefficients so obtained are tabulated in Table I. The third virial coefficients are plotted in Figure 6, and the arithmetic average fourth virial coefficients in Figure 7, as functions of temperature. Significant differences exist in the values of C determined by the two treatments, and the smoothed curve in Figure 6 compromises between the two sets of values. The final values of B, C, and D, smoothed with respect to temperature (Figures 6 and 7) are presented in Table II. Uncertainties associated with these values are discussed in a later section.

Neopentane. Twenty of the Burnett apparatus runs with neopentane reported by Heichelheim and coworkers (*8*)

Table I. Results of Analysis of the Isopentane Data of Silberberg, McKetta, and Kobe (*11*)

Temp., °C.	Run No.	First Residual Analysis: ρ_0 (Mole/Liter) (*11*)	First Residual Analysis: ρ_0 (Mole/Liter) This work	First Residual Analysis: $-B$, (liter/g. mole)	First Residual Analysis: C, (liter/g. mole)^2	Second Residual Analysis: C, (liter/g. mole)^2	Second Residual Analysis: D, (liter/g. mole)^3
50	20	0.07815	0.07812	0.9581	0.5059	...	...
50	21	0.05810	0.05809	0.9579	0.5059	...	...
75	23	0.13696	0.13687	0.7715	0.3647	...	...
75	24	0.12286	0.12285	0.7715	0.3645	...	...
100	25	0.26148	0.26138	0.6427	0.2389	0.2320	−0.720
100	26	0.22226	0.22216	0.6427	0.2389	0.2320	−0.801
100	27	0.27488	0.27488	0.6427	0.2388	0.2320	−0.724
125	28	0.46926	0.46891	0.5579	0.1557	0.1496	−0.198
125	29	0.42392	0.42392	0.5579	0.1557	...	...
125	30	0.38357	0.38342	0.5579	0.1557	0.1496	−0.220
150	31	0.78640	0.78620	0.4799	0.0959	...	...
150	32	0.68553	0.68533	0.4800	0.0959	0.0983	−0.0545
150	33	0.61674	0.61634	0.4800	0.0960	0.0983	−0.0534
175	34	1.4348	1.4340	0.4208	0.0705	...	...
175	35	1.2434	1.2430	0.4208	0.0706	0.0675	−0.0153
175	36	1.4739	1.4731	0.4209	0.0706	0.0675	−0.0147
188.5	41	4.8399	4.8379	0.3882	0.0555	0.0525	0.00054
188.5	42	4.6168	4.6148	0.3882	0.0555	0.0525	0.00054
200	37	5.2308	5.2298	0.3663	0.0508	0.0507	0.00056
200	38	4.6584	4.6564	0.3662	0.0508	0.0507	0.00056
200	38A[a]	0.82101	0.82066	0.3661	0.0508	...	...

[a] Run No. 38A consists of the last nine points of run No. 38, treated as a separate run.

Table II. Smoothed Virial Coefficients of Isopentane

Temp., °C.	$-B$, (Liter/G. Mole)	C, (Liter/G. Mole)^2	D, (Liter/G. Mole)^3
0	(1.3706)	...	...
25	(1.1497)	...	...
50	0.9540	0.506	...
75	0.7752	0.364	...
100	0.6429	0.239	−0.748
125	0.5557	0.151	−0.209
150	0.4825	0.097	−0.054
175	0.4191	0.067	−0.015
188.5	0.3884	0.056	0.001
200	0.3664	0.049	0.002

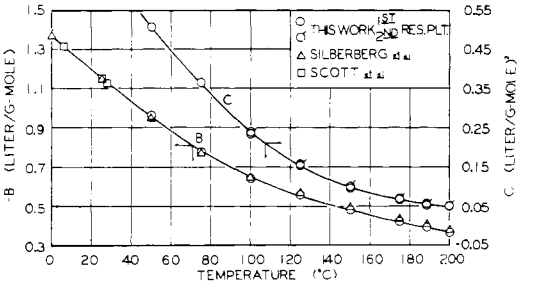

Figure 6. Second and third virial coefficients of isopentane

were also analyzed. The temperature range of these runs was from 30° to 200° C. and included two runs at 161.5° C., slightly greater than the critical temperature. As with the isopentane, the data were analyzed according to Equation 17 (Figure 3). The apparatus constants used were those reported by Heichelheim (Table III). Results for the second and third virial coefficients from runs at the same temperature were less consistent than for isopentane (Table IV), and in general, scattering of the data points on the residual plots was more severe. Arithmetic average values of the second and third virial coefficients of neopentane are shown as functions of temperature (Figure 8), from which were read the smoothed values (Table V). Uncertainties associated with the values in Table V are discussed in the next section.

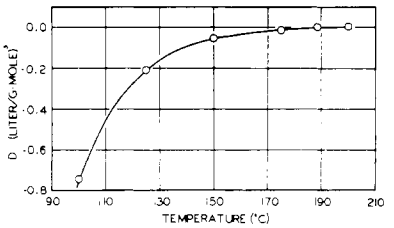

Figure 7. The fourth virial coefficient of isopentane

Table III. Burnett Apparatus: The University of Texas Helium Calibration Data of Heichelheim

Run No. 2, Nov. 60

R	P(R)[a]
0	63.090
1	55.975
2	49.676
3	44.076
4	39.110
5	34.713
6	30.809
7	27.334
8	24.260
9	21.526
10	19.100
11	16.952

Run No. 3 Nov. 60

R	P(R)
0	59.079
1	52.389
2	46.485
3	41.243
4	36.588
5	32.482
6	28.815
7	25.583
8	22.699
9	20.150
10	17.878
11	15.869

Run No. 4 Dec. 60

R	P(R)
0	61.407
1	43.332
2	30.581
3	21.578

Run No. 5 Dec. 60

R	P(R)
0	56.699
1	39.980
2	28.237
3	19.924

Run No. 6 Dec. 60

R	P(R)
0	60.141
1	42.436
2	29.941
3	21.134

Run No. 7 Dec. 60

R	P(R)
0	1003.628
1	888.264
2	786.314
3	696.289
4	616.687
5	566.329

Run No. 7 Dec. 60 Cont.

R	P(R)
6	484.086
7	429.000
8	380.332
9	337.155
10	298.928
11	265.060
12	235.091
13	208.482
14	184.922
15	164.005
16	145.516
17	129.113
18	114.517
19	101.602
20	90.216
21	80.000
22	70.988
23	62.985
24	55.905
25	49.616
26	44.017
27	39.059
28	34.660
29	30.758
30	27.298
31	24.226
32	21.504
33	19.082
34	16.930

Run No. 8 Dec. 60

R	P(R)
0	746.953
1	661.470
2	585.941
3	519.129
4	460.036
5	407.710
6	361.484
7	320.469
8	284.122
9	251.967
10	223.468
11	198.213
12	175.869
13	156.001
14	138.372

Run No. 9 Dec. 60

R	P(R)
0	118.866
1	105.479
2	93.580
3	83.038
4	73.678
5	65.401
6	58.017

Run No. 9 Dec. 60 Cont.

R	P(R)
7	51.496
8	45.706
9	40.551
10	35.981
11	31.930
12	28.330
13	25.144
14	22.316
15	19.797
16	17.570

Run No. 10 Dec. 60

R	P(R)
0	1003.799
1	703.538
2	494.166
3	347.628
4	244.828
5	172.518
6	121.696
7	85.825
8	60.574
9	42.751
10	30.164
11	21.287

Run No. 11 Dec. 60

R	P(R)
0	861.591
1	604.459
2	424.885
3	299.076
4	210.663
5	148.491
6	104.711
7	73.896
8	52.156
9	36.797
10	25.966

Run No. 12 Dec. 60

R	P(R)
0	958.373
1	958.373
2	472.026
3	332.118
4	233.920
5	164.858
6	116.241
7	82.001
8	57.877
9	40.849
10	28.819

Run No. 13 Dec. 60

R	P(R)
0	927.395

Run No. 13 Dec. 60 Cont.

R	P(R)
1	650.299
2	456.966
3	321.558
4	226.491
5	159.638
6	112.568
7	79.386
8	56.052
9	39.566
10	27.912

Run No. 14 Dec. 60

R	P(R)
0	779.753
1	547.374
2	384.920
3	271.019
4	190.968
5	134.638
6	94.964

Run No. 15 Mar. 61

R	P(R)
0	931.969
1	827.127
2	734.323
3	652.054
4	579.144
5	514.526
6	457.184
7	406.294
8	361.123
9	320.997
10	285.333
11	253.698
12	225.617
13	200.623
14	178.455
15	158.664
16	141.126
17	125.519
18	111.655
19	99.315
20	88.385
21	78.595
22	69.916
23	62.223
24	55.373
25	49.267
26	43.826
27	38.986
28	34.688
29	30.852
30	27.456
31	24.429
32	21.730
33	19.342
34	17.203

Run No. 16 Mar. 61

R	P(R)
0	740.165
1	519.708
2	365.559
3	257.422
4	181.380
5	127.902
6	90.218
7	63.659
8	44.922
9	31.714
10	22.381

Run No. 17 Mar. 61

R	P(R)
0	1245.182
1	871.260
2	611.230
3	429.658
4	302.433
5	213.034
6	150.152
7	105.884
8	74.668
9	52.731
10	37.213
11	26.255

Run No. 18 July 61

R	P(R)
0	1154.490
1	1028.690
2	916.580
3	817.029
4	728.519
5	649.616
6	579.388
7	516.749
8	461.034
9	411.321
10	367.035
11	327.501
12	292.341
13	260.924
14	232.881
15	207.874
16	185.556
17	165.611
18	147.866
19	132.001
20	117.889
21	105.229
22	93.959
23	83.888
24	74.932
25	66.922
26	59.791

Run No. 18 July 61 Cont.

R	P(R)
27	53.383
28	47.672
29	42.576
30	38.015
31	33.951
32	30.307
33	27.062
34	24.167
35	21.585
36	19.276
37	17.217

Run No. 19 July 61

R	P(R)
0	1021.400
1	717.879
2	505.376
3	356.213
4	251.268
5	177.327
6	125.193
7	88.396
8	62.498
9	44.166
10	31.202
11	22.048

Run No. 20 July 61

R	P(R)
0	914.477
1	643.073
2	452.912
3	319.321
4	225.268
5	159.011
6	112.288
7	79.288
8	56.035
9	39.593
10	27.987

Run No. 21 July 61

R	P(R)
0	817.743
1	575.402
2	405.405
3	285.905
4	201.780
5	142.409
6	100.547
7	71.041
8	50.204
9	35.487
10	25.074

[a] $P(R)$ = pressure in pounds per square inch after rth expansion.

Table IV. Results of First Residual Analysis for Neopentane[a]

Temp., °C.	Run No.	ρ_0 (G. Mole/Liter) (8)	ρ_0 (G. Mole/Liter) This work	$-B$, (Liter/G. Mole)	C, (Liter/G. Mole)^2
30	1	0.07050	0.07045	0.9003	0.2817
30	2	0.08108	0.08104	0.9004	0.2818
50	3	0.14473	0.14463	0.7672	0.1491
50	4	0.13902	0.13882	0.7613	0.1518
75	5	0.15125	0.15095	0.6320	0.1087
75	6	0.09414	0.09406	0.6444	0.1057
75	7	0.26310	0.26275	0.6314	0.1043
75	8	0.26447	0.26417	0.6410	0.1060
100	9	0.45727	0.45727	0.5499	0.0918
100	10	0.43695	0.43675	0.5496	0.0920
125	11	0.79978	0.79918	0.4783	0.0821
125	12	0.76587	0.76457	0.4781	0.0823
150	13	1.4476	1.4447	0.4168	0.0690
150	14	1.4808	1.4776	0.4167	0.0690
161.5	15	4.4470	4.4347	0.3845	0.0542
161.5	16	5.7693	5.7603	0.3844	0.0543
175	17	5.4212	5.4152	0.3577	0.0510
175.	18	4.4885	4.4810	0.3577	0.0511
200	19	1.6599	1.6509	0.3185	0.0463
200	20	1.6673	1.6563	0.3175	0.0463

[a] Based on the data of Heichelheim and coworkers (8).

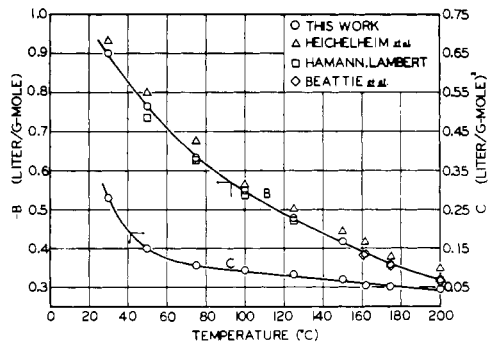

Figure 8. The virial coefficients of neopentane

Table V. Smoothed Virial Coefficients of Neopentane

Temp., °C.	$-B$, (Liter/G. Mole)	C, (Liter/G. Mole)^2
30	0.9004	0.282
50	0.7640	0.151
75	0.6372	0.108
100	0.5487	0.091
125	0.4775	0.077
150	0.4135	0.065
161.5	0.3864	0.059
175	0.3577	0.054
200	0.3180	0.044

Also shown in Figure 8 are the values of B derived from the same data by Heichelheim *et al.* (8), using extrapolations of isothermal graphs of $z - 1/p$ *vs.* pressure. The smoothed results of the new method of analysis for B are consistently lower than those from the earlier treatment by from 18 to 42 ml. per gram mole and are in much better agreement with the values reported by Hamann and Lambert (7) and by Beattie, Douslin, and Levine (1) (Figure 8).

Table IV also presents a comparison of the values of initial density ρ_0 determined in this work with those reported by Heichelheim and coworkers (8), which were determined as intercepts from large-scale Berlin-type plots of the low-pressure data. Deviations between the two sets of data, excluding the 200° C. runs, are less than 0.3%, with an average deviation of 0.13%. Values of ρ_0 from the new analysis are consistently lower. The two runs at 200° C., which could be treated by the first residual method, gave values of ρ_0 lower by 0.54 and 0.66%, respectively, than those reported by Heichelheim. Apparently, the most probable reason for this discrepancy is a systematic error in the low-pressure measurements at this temperature, possibly resulting indirectly from an accident with the apparatus which required recalibration of the apparatus constants with helium. Compressibility factors reported in the earlier paper would therefore seem to be too high by as much as 0.3% and at 200° C. by as much as 0.6%.

An attempt was made to analyze the neopentane data by the second residual method to yield values of the fourth virial coefficient. Unfortunately, the precision of the data did not warrant this treatment.

SOURCES OF ERROR

Because of the graphical smoothing performed for each run and the averaging and subsequent smoothing of virial coefficients with respect to temperature, random errors in pressure and temperature measurements would seem to have little effect upon the final smoothed values of the virial coefficients. Therefore, only systematic errors would be likely to affect the results in this new method of analysis. The following are the sources of such errors: systematic temperature errors—negligible because of the relatively small effect of temperature on B, C, and D; systematic pressure errors—believed to be less than 0.04% of the pressure; and apparatus constant errors—believed to be less than 0.01%.

Because of the nature of the residuals used here, the effect of systematic errors in pressure may be considerably cancelled by adjustment of the value of initial density ρ_0 to result in a more linear graph at low densities, an adjustment which is of course intrinsic in the method. It is therefore conceivable that such errors may result in erroneous values of initial density but nonetheless relatively accurate values of B, C, and possibly even D. The effect of systematic errors in pressure was not studied in detail in this investigation, but a preliminary analysis indicated that the estimated maximum error of 0.04% in pressure should not introduce an error greater than 0.4% in B or 1% in C. The effect on D cannot be realistically evaluated because of the lack of precision in the data. A detailed analysis of the effect of this source of error is planned, using a computer program presently under development.

The effect of a systematic error in the apparatus constant was studied for run No. 38 with isopentane at 200° C. (11) (Table VI). This run was selected because of the precision of pressure measurements, including the lower pressure points. Values of N, reported by the original investigators (10) to be 1.41507, were varied from 1.41460 to 1.41580, a change from −0.033% to +0.052%. Values of ρ_0, B, and C were graphically determined by the first residual method for each value of N. Extreme errors in N caused a curvature too great to be corrected by adjustment of ρ_0. The limits over which N could be varied without clearly revealing the presence of systematic error were from 1.41490

Table VI. Effect of Apparatus Constants on Virial Coefficients[a]

	First Residual Analysis			Second Residual Analysis	
N	ρ_0, (g. mole/liter)	$-B$, (liter/g. mole)	C, (liter/g. mole)^2	C, (liter/g. mole)^2	D, (liter/g. mole)^3
1.41460	4.6384	0.3615	0.0485	...	...
1.41490	4.6494	0.3638	0.0494	0.0482	0.00110
1.41507	4.6564	0.3662	0.0508	0.0507	0.00056
1.41560	4.6764	0.3690	0.0523	0.0519	0.00006
1.41580	4.6844	0.3712	0.0538	...	...

[a] Isopentane at 200° C., run No. 38, data of Silberberg, McKetta, and Kobe (11).

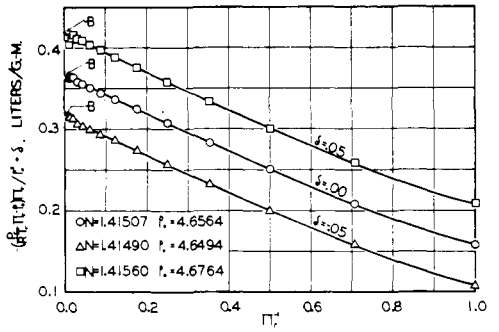

Figure 9. The effect of the apparatus constant on the virial coefficients of isopentane at 200° C.

Run No. 38, data of Silberberg (*11*)

to 1.41560. The first residual plots, with the curves displaced for clarity, for these two values as well as for the assumed correct value (1.41507) are shown in Figure 9.

The effect of the variation in N on the results of the second residual method was also explored for run No. 38 (Table VI). Values of ρ_0 and B determined from the first residual plot for each value of N were used. For this set of data, the second residual plot gave greater errors in the third virial coefficient when N was too low and the first residual plot gave the greater errors in C when N was too high. The fourth virial coefficient of isopentane is so small at 200° C. that it is tremendously sensitive to such errors in N, varying in this case by an order of magnitude. The absolute variation in D, however, was relatively small.

Silberberg, Kobe, and McKetta (*10*) stated a 95% probability that the apparatus constant determined by them was accurate to 0.01%. Heichelheim and coworkers (*8*) made no estimate of apparatus constant accuracies, but they are believed to be comparable. On the basis of this admittedly incomplete analysis, the authors estimated that apparatus constant uncertainties do not introduce errors in B greater than 1% and errors in C greater than 0.001 (liter per gram mole)^2, or about 2%. The effect on D of errors in N could not be generalized from this brief analysis.

Over-all accuracies in virial coefficients are always difficult to estimate realistically. Certainly the temptation must be avoided to base such an estimate on reproducibility at a given temperature, as subsequent smoothing with respect to temperature may indicate that the reproducible value at that temperature was probably in error. Although the effects of systematic errors in pressure and in apparatus constant are believed to be greatly minimized in the Burnett data as analyzed here, the complicated interaction of the parameters in the first and second residuals, along with the fact that the virial coefficients are evaluated as limits, make virtually impossible any absolute statements in regard to accuracies of the virial coefficients. The errors in the second virial coefficient B at the experimental temperatures reported in Tables II and V are believed not to exceed 2%. Values reported at the higher temperatures are probably more accurate than this estimate. Errors in the third virial coefficient C are believed to be less than 5% or 0.002 (liter per gram mole)^2, whichever is the greater. Errors in the fourth virial coefficient D probably do not exceed 10% or 0.002 (liter per gram mole)^3, whichever is the larger.

APPENDIX

Evaluation of Apparatus Constant. The singular importance of the Burnett apparatus constant is readily apparent from the relations developed here. When the number of expansions to low pressure is ten or more, an apparatus constant error no greater than 0.01% will introduce a maximum error in the compressibility factor data of 0.1% or more. For over-all accuracies of 0.05%, the uncertainty in N must be reduced to only a few parts in 100,000. Modern high-speed digital computers make it possible to process the experimental data from a single run according to Equation 12 to yield least-squares values of the zero-pressure apparatus constant N_∞ as well as ρ_0 and the virial coefficients. Unfortunately, the results from such an analysis will be dependent upon the point of truncation of the equation. A residual type of graphical analysis which could eliminate the truncation problem and at the same time provide high sensitivity to small changes in N (or N_∞) would have an obvious advantage, even though it might suffer from less objectivity than the impersonal least-squares procedures.

Such a residual method was developed by Butcher and Dadson (*3*) and is the basis of Equations 14 through 16 presented here. This method has the advantage of operating directly on the experimental pressures and temperatures. Another residual method for testing the apparatus constant, similarly based upon the Leiden virial equation of state, was presented by Canfield and coworkers (*4, 5*). This method is based upon the graph of the residual function $V(z-1)$ *vs.* $1/V$. To prepare such a graph for each trial value of N_∞ requires that a value of ρ_0 be obtained from the data for each N_∞, the value of z_r calculated from the rearrangement of Equation 5, V_r calculated for each point, and the graph of $V_r(z_r - 1)$ *vs.* $1/V_r$ be prepared. Since theory predicts this graph to approach linearity as $1/V_r$ approaches zero, the error in the assumed value of N_∞ is revealed in excessive curvature at low densities.

The authors desired to test the sensitivity of the residual method for determining N_∞ represented by Equation 15 and at the same time compare the method with the more laborious graphical technique of Canfield and coworkers (*4, 5*). Consequently, the same data set was chosen as was used by Canfield *et al.* to illustrate their method. The data were obtained with helium at −90° C. and extended from about 524 atm. to slightly less than 3 atm., involving a total of 13 experimental points (12 expansions). For convenience, Equation 15 was rewritten in a pressure-ratio form. As experimental temperatures were controlled to within ± 0.002° C., the temperature ratio has been omitted.

$$p_{r-1}N^{r}\left(1 - N\frac{p_r}{p_{r-1}}\right) = BRTN(N-1)\rho_0^2 + CRTN(N^2-1)\rho_0^3N^{-r} + DRTN(N^3-1)\rho_0^4N^{-2r} + \ldots \qquad (29)$$

The residual graphs are shown in Figure 10 for four equally spaced values of N_∞ from 1.49900 to 1.49930; the curves are displaced by arbitrary amounts for the sake of clarity. The apparatus constant applicable to each expansion (N_r) was calculated from N_∞ using the equation presented by references (*4, 5*) and employed in the ordinate

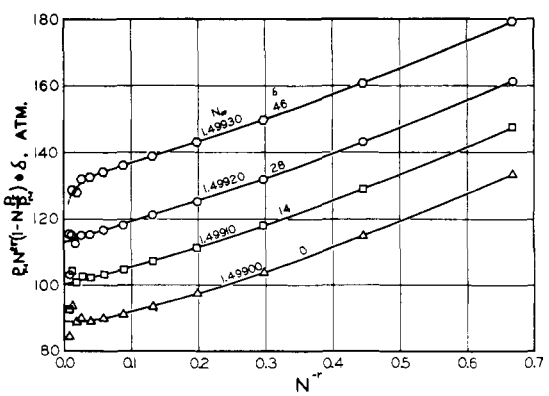

Figure 10. Residual test of apparatus constant

Helium at −90° C., data of Canfield (*4*)

of Figure 10. The effect of this nonconstant apparatus "constant" in these graphs is to introduce slightly greater curvature at the high density end than would exist if N_r were truly constant. After the first three points, however, the effect is entirely negligible.

Figure 10 shows readily that the value 1.49930 is too great. It is less obvious that the value 1.49900 is too small, but the tendency toward upward curvature of the low-density data points is clearly in evidence. On a large-scale plot, the curve for 1.49920 exhibits greater linearity at low densities than does that for 1.49910, but to prefer one over the other presumes knowledge of how rapidly the graph should approach linearity as the density decreases. On the basis of this figure, one might choose the value $N_\infty = 1.49915$ as best. In Figure 10, the lowest-density point, which deviates markedly from the data trend except when N_∞ is too great, actually represents a deviation in the pressure ratio p_r/p_{r-1} of less than 0.01%.

In their analysis of the same data, Canfield and coworkers (*4*, *5*) apparently omitted from consideration the four low-pressure points (less than 14 atm.) and did not plot the three high-pressure points (above 190 atm.), although they stated that the variation of $V(z-1)$ with $1/V$ "is essentially linear" between 50 and 500 atm. (*5*). From their graphs, they were able to determine that the value of 1.49910 was too small and that 1.49920 was too large, selecting $N_\infty = 1.49918$ as the best value. This value agrees within 0.002% with the value estimated above from the curves of Figure 10.

In conclusion, with sufficiently precise helium calibration data, the residual method illustrated in Figure 10 should be capable of determining the apparatus constant within $\pm 0.005\%$. The method of Canfield *et al.* (*4*, *5*) apparently is more sensitive and inherently will involve less data scatter, as each point is based upon a single pressure measurement rather than two, but requires considerably more data processing. Probably the most sensitive criterion for determining the apparatus constant would be the low-density linearity of the graph of $V_r(z_r - 1)$ *vs.* $1/V_r$, with ρ_0 being determined for each trial value of N_∞ by the trial-and-error first-residual procedure described earlier in this paper.

NOMENCLATURE

B = second virial coefficient, liter per gram mole
B' = coefficient of p in Berlin Equation 8, atm.$^{-1}$
C = third virial coefficient, (liter per gram mole)^2
C' = coefficient of p^2 in Berlin Equation 8, atm.$^{-2}$
D = fourth virial coefficient, (liter per gram mole)^3
D' = coefficient of p^3 in Berlin Equation 8, atm.$^{-3}$
N = apparatus constant; ratio of system volumes after and before expansion
N_r = apparatus constant applicable to rth expansion
N_∞ = apparatus constant at zero pressure
p = absolute pressure, atm.
R = gas constant, 0.0820544 (liter)(atm.)/(gram mole)(° K.)
T = absolute temperature, ° K.
V = molal volume, liter per gram mole
z = compressibility factor = pV/RT

$\pi_r = \prod_{i=1}^{r} N_i = N_1 N_2 \ldots N_r$

ρ = molal density, gram mole per liter
ρ_0 = initial molal density, gram mole per liter

Subscripts

f = state of system after final expansion
r = state of system after rth expansion
$r-1$ = state of system before rth expansion
0 = initial state of system

LITERATURE CITED

(1) Beattie, J.A., Douslin, D.R., Levine, S.W., *J. Chem. Phys.* **20**, 1619 (1952).
(2) Burnett, E.S., *J. Appl. Mech.* **58**, A136 (1936).
(3) Butcher, E.G., Dadson, R.S., *Proc. Roy. Soc. (London)* **A277**, 448 (1964).
(4) Canfield, F.B., Jr., Ph.D. thesis, Rice University, Houston, Tex., May 1962.
(5) Canfield, F.B., Jr., Leland, T.W., Kobayashi, R., "Advances in Cryogenic Engineering 8," pp. 146–57, Plenum Press, New York, 1963.
(6) Cook, D., *Can. J. Chem.* **35**, 268 (1957).
(7) Hamann, S.D., Lambert, J.A., *Australian J. Chem.* **7**, 1 (1954).
(8) Heichelheim, H.R., Kobe, K.A., Silberberg, I.H., McKetta, J.J., J. CHEM. ENG. DATA **7**, 507 (1962).
(9) Scott, D.W., McCullough, J.P., Williamson, K.D., Waddington, G., *J. Am. Chem. Soc.* **73**, 1707 (1951).
(10) Silberberg, I.H., Kobe, K.A., McKetta, J.J., J. CHEM. ENG. DATA **4**, 314 (1959).
(11) Silberberg, I.H., McKetta, J.J., Kobe, K.A., *Ibid.*, **4**, 323 (1959).
(12) Yntema, J.L., Schneider, W.G., *J. Chem. Phys.* **18**, 641 (1950).

RECEIVED for review November 11, 1966. Accepted February 17, 1967. This research was supported in part by the National Science Foundation.